A Modified Discontinuous Galerkin Method for Solving Efficiently Helmholtz Problems

Magdalena Grigoroscuta-Strugaru[1,2], Mohamed Amara[1],
Henri Calandra[3] and Rabia Djellouli[4,*]

[1] *INRIA Bordeaux Sud-Ouest Research Center, Team Project Magique-3D and LMA/CNRS UMR 5142, Université de Pau et des Pays de l'Adour, France.*
[2] *BCAM, Basque Center for Applied Mathematics, Bilbao, Spain.*
[3] *TOTAL, Avenue Larribau, Pau, France.*
[4] *Department of Mathematics, California State University Northridge and Interdisciplinary Research Institute for the Sciences, IRIS, USA.*

Abstract. A new solution methodology is proposed for solving efficiently Helmholtz problems. The proposed method falls in the category of the discontinuous Galerkin methods. However, unlike the existing solution methodologies, this method requires solving (a) *well-posed* local problems to determine the primal variable, and (b) a global positive *semi-definite Hermitian* system to evaluate the Lagrange multiplier needed to restore the continuity across the element edges. Illustrative numerical results obtained for two-dimensional interior Helmholtz problems are presented to assess the accuracy and the stability of the proposed solution methodology.

1 Introduction

The Helmholtz equation belongs to the classical equations of mathematical physics that are well understood from a mathematical view point. However, the numerical approximation of the solution is still a challenging problem in spite the tremendous progress made during the past fifty years (see, for example, the recent monograph [18] and the

---

*Corresponding author. *Email addresses:* magdalena.grigoroscuta@univ-pau.fr (M. Grigoroscuta-Strugaru), mohamed.amara@univ-pau.fr (M. Amara), henri.calandra@total.com (H. Calandra), rabia.djellouli@csun.edu (R. Djellouli)

references therein). Indeed, the standard finite element method (FEM) is not well suited for solving Helmholtz problems in the mid- and high-frequency regime because of the quasi-optimality constant which grows with the wavenumber k, as explained in details in [5]. In order to maintain a certain level of accuracy while increasing the frequency, a mesh refinement is required and/or higher order FEM are used, leading to a prohibitive computational cost for high wavenumbers.

In response to this challenge, alternative techniques were proposed. Numerous of these approaches use the plane waves, since they are expected to better approximate highly oscillating waves [4,6–12,19,20,23]. In the discontinuous Galerkin method (DGM) designed by Farhat *et al.* and presented in a series of papers [8–10], the solution is approximated at the element mesh level using a superposition of plane waves which results in a discontinuous solution along interior boundaries of the mesh. The continuity is then restored weakly with Lagrange multipliers. The rectangular and quadrilateral elements constructed in [8–10] clearly outperform the standard Galerkin FEM. For example, for $ka \geq 10$ and for a fixed level of accuracy, the so-called *R*-4-1 element reduces the total number of degrees of freedom (dofs) required by the *Q*1 finite element by a factor greater or equal to five. Similar results are obtained for the *R*-8-2a and *R*-8-2b elements when compared to the *Q*2 element, and for *Q*-16-4 and *Q*-32-8 when compared to the *Q*4 element. In spite of this impressive performance, the DGM has three important drawbacks. First, the method has to satisfy an *inf-sup* condition which is translated, in practice, as a compatibility requirement: the number of dofs of the Lagrange multiplier (corresponding to the dual variable) and of the field (the primal variable) cannot be chosen arbitrarily. The problem here is that there is no theoretical result on how to satisfy this compatibility requirement, except for the simple case of *R*-4-1 element (see [2]). Hence, for other elements, the existing choices are based on numerical experiments only. The second major issue with the DGM is that it becomes unstable as we refine the mesh [1]. Such instabilities occur because of the singularity of the local problems and, to some extent, to the loss of the linear independence of the plane waves as the step size mesh discretization tends to zero. The latter affects dramatically the stability of the global system due to its ill-conditioning nature. Finally, the DGM exhibits a loss of accuracy for unstructured mesh [9].

We propose a new solution methodology for Helmholtz problems, that falls in the category of discontinuous Galerkin methods. The proposed formulation distinguishes itself from existing procedures by the *well-posed* character of the local problems and by the resulting global system which is associated with a positive *semi-definite Hermitian* matrix. More specifically, the computation domain is subdivided in quadrilateral- or triangular-shaped elements. The solution is approximated, at the element level, by a superposition of plane waves that are solution of the Helmholtz equation. The continuity of the solution at the interior interfaces of the elements is then enforced by Lagrange multipliers. Unlike the DGM, the proposed method does not require the continuity of the normal derivative. Consequently, Lagrange multipliers are introduced to restore, in a weak sense, the continuity of both the field and its normal derivative across interior boundaries of the mesh.

Such choice leads to solving (a) local boundary value problems that are well posed in the sense of Hadamard [15] and (b) a global Hermitian system, whose unknowns are the Lagrange multipliers. Note that the proposed technique is a two-step procedure where the local problems are first solved and then the Lagrange multipliers are evaluated. This two-step approach allows us to consider equally structured and unstructured meshes with either triangular- or quadrilateral-shaped elements. Since the proposed solution methodology resembles in some aspect the DGM, we will refer to it as mDGM (*m*odified *D*iscontinuous *G*alerkin *M*ethod).

2 Preliminaries

We consider the following class of waveguide-type problems:

$$(\text{BVP}) \begin{cases} -\Delta u - k^2 u = f, & \text{in } \Omega, \\ \partial_n u = iku + g, & \text{on } \partial\Omega, \end{cases}$$

where $\Omega \subset \mathbb{R}^2$ is an open bounded region, with smooth boundary $\partial\Omega$. k is a positive number representing the wavenumber. ∂_n is the normal derivative in the outgoing direction on $\partial\Omega$. f and g are complex valued functions such that $f \in L^2(\Omega)$ and $g \in L^2(\partial\Omega)$. The second equation of BVP is a representation of a class of non-homogeneous Robin boundary conditions, but other types of boundary condition can be considered.

Note that BVP is considered here for its simplicity since it allows us to compute analytically the solution u for a suitable choice of Ω, f and g. Such an expression of u is used when assessing the accuracy of mDGM.

Let τ_h be a regular triangulation of Ω into quadrilateral- or triangular-shaped subdomains K whose boundaries are denoted by ∂K. The mesh discretization step size is denoted by h. We introduce the space of the primal variable:

$$\mathcal{V} = \left\{ v \in L^2(\Omega) ; \, v|_K \in H^1(K) \right\}.$$

For any $v \in \mathcal{V}$, we define the jump across an interior edge $e = \partial K \cap \partial K'$ by:

$$[v] = v^K - v^{K'}.$$

We introduce the space of the dual variable, corresponding here to Lagrange multipliers, by:

$$\mathcal{M} = \left\{ \mu \in \prod_{K \in \tau_h} L^2(\partial K) ; \, \mu = 0 \text{ on } \partial K \cap \partial\Omega \right\}.$$

For any function $\mu \in \mathcal{M}$, we define the jump across an interior edge $e = \partial K \cap \partial K'$ by:

$$[[\mu]] = \mu^K + \mu^{K'}.$$

3   The continuous approach

The basic idea of mDGM is to evaluate u, the solution of BVP, using the following splitting:

$$u = \Phi(\lambda) + \varphi, \tag{3.1}$$

where φ and Φ are elements of $\mathcal{V}$ and λ is an element of $\mathcal{M}$. φ can be viewed as a local lifting of the problem's data, whereas $\Phi(\lambda)$ is the contribution of the Lagrange multipliers, introduced to restore the continuity. We then proceed into the following two steps to compute these three quantities:

Step 1: For all $K \in \tau_h$ and $\mu \in \mathcal{M}$, we compute φ and $\Phi(\mu)$. This is achieved by solving local Helmholtz problems. This step is called the restriction procedure.

Step 2: We determine $\lambda \in \mathcal{M}$ by solving a global linear system to ensure the continuity in a weak sense of the solution u given by (3.1) and of its normal derivative. This step is called the optimization procedure.

3.1   Step 1: The restriction procedure

As stated earlier, this step is devoted to the computation of φ and $\Phi(\mu)$, for all $\mu \in \mathcal{M}$, by solving locally Helmholtz problems. More specifically, for all $K \in \tau_h$, we compute φ^K by solving the following boundary value problem:

$$(\text{BVP1}) \begin{cases} \text{Find } \varphi^K \in H^1(K) \text{ such that:} \\ -\Delta\varphi^K - k^2\varphi^K = f, & \text{in } K, \\ \partial_n\varphi^K = ik\varphi^K + g, & \text{on } \partial K \cap \partial\Omega, \\ \partial_n\varphi^K = i\alpha\varphi^K, & \text{on } \partial K \cap \Omega. \end{cases}$$

Next, for all $\mu \in \mathcal{M}$ and $K \in \tau_h$, we compute $\Phi(\mu^K)$ by solving the boundary value problem given by:

$$(\text{BVP2}) \begin{cases} \text{Find } \Phi(\mu^K) \in H^1(K) \text{ such that:} \\ -\Delta\Phi(\mu^K) - k^2\Phi(\mu^K) = 0, & \text{in } K, \\ \partial_n\Phi(\mu^K) = ik\Phi(\mu^K), & \text{on } \partial K \cap \partial\Omega, \\ \partial_n\Phi(\mu^K) = i\alpha\Phi(\mu^K) + \mu^K, & \text{on } \partial K \cap \Omega, \end{cases}$$

with $\alpha \in \mathbb{R}_+^*$.

Remark 3.1. *(i)* The presence of $\alpha \in \mathbb{R}_+^*$ ensures the uniqueness of the solution of BVP1 and BVP2, as established in [3] and [13]. The numerical results reported in this paper were obtained for $\alpha = k$.

(ii) Since $f \in L^2(\Omega)$ and $g \in L^2(\partial\Omega)$, it follows from the standard regularity results for Laplace's operator [14] that $\partial_n \varphi^K \in L^2(\partial K)$ and $\partial_n \Phi(\mu^K) \in L^2(\partial K)$ for all $\mu \in \mathcal{M}$. For more details, we refer the reader to see Theorem 1 and Remark 1 on p. 1044 in [2].

It is easy to verify that the variational formulation of both problems can be expressed in a compact form as follows:

$$\begin{cases} \text{Find } \Psi^K \in H^1(K) \text{ such that:} \\ a_K\left(\Psi^K, v^K\right) = L_K\left(v^K\right), \quad \forall v^K \in H^1(K), \end{cases} \tag{3.2}$$

where $a_K(\cdot, \cdot)$ is a bilinear form given by:

$$a_K\left(w^K, v^K\right) = \int_K \nabla w^K \cdot \nabla \overline{v^K} dx - k^2 \int_K w^K \overline{v^K} dx - i\alpha \int_{\partial K \cap \Omega} w^K \overline{v^K} ds$$

$$- ik \int_{\partial K \cap \partial\Omega} w^K \overline{v^K} ds, \quad \forall w^K, v^K \in H^1(K). \tag{3.3}$$

We have:

$$\varphi^K = \Psi^K \quad \text{when} \quad L_K\left(v^K\right) = \int_K f \overline{v^K} dx + \int_{\partial K \cap \partial\Omega} g \overline{v^K} ds, \tag{3.4}$$

and for each $\mu \in \mathcal{M}$:

$$\Phi\left(\mu^K\right) = \Psi^K \quad \text{when} \quad L_K\left(v^K\right) = \int_{\partial K \cap \Omega} \mu^K \overline{v^K} ds. \tag{3.5}$$

Next, we define φ such that, for all element K in the mesh, the restriction of φ to K is φ^K, i.e. $\varphi|_K = \varphi^K$. Similarly, for all element K and for all μ in $\mathcal{M}$, we define $\Phi(\mu)$ such that we have $\Phi(\mu)|_K = \Phi\left(\mu^K\right)$. Using the definition of φ and $\Phi(\mu)$, we have:

$$\varphi \in \mathcal{V} \quad \text{and} \quad \Phi(\mu) \in \mathcal{V}, \quad \forall \mu \in \mathcal{M}.$$

In summary, Step 1 allows us to compute, for all μ in $\mathcal{M}$:

$$\varphi + \Phi(\mu) \in \mathcal{V} \tag{3.6}$$

by solving one variational problem given by (3.2) with different right-hand side given by (3.4) and (3.5). Step 1 can be viewed, to some extent, as a prediction step.

3.2 Step 2: The optimization procedure

From BVP1 and BVP2, it is easy to observe that for each $K \in \tau_h$, the function $\varphi^K + \Phi\left(\mu^K\right)$ satisfies locally both equations of BVP. This justifies Eq. (3.1). To write the first equation of BVP in Ω, we need to ensure that for some $\lambda \in \mathcal{M}$, we have $\varphi + \Phi(\lambda) \in H^1(\Omega)$ and its normal derivative is continuous across the interior edges. This requirement can be

viewed as a correction procedure since we select the best-fit Lagrange multiplier λ. The determination of λ is accomplished by solving the following global variational problem:

$$(VF)\begin{cases} \text{Find } \lambda \in \mathcal{M} \text{ such that} \\ A(\lambda,\mu) = F(\mu), \quad \forall \mu \in \mathcal{M}, \end{cases} \tag{3.7}$$

where the bilinear form $A(\cdot,\cdot)$ is given by:

$$A(\eta,\mu) = \sum_{e\text{-interior edge}} \beta_e \int_e [\Phi(\eta)]\overline{[\Phi(\mu)]}ds + \sum_{e\text{-interior edge}} \gamma_e \int_e [[\partial_n\Phi(\eta)]]\overline{[[\partial_n\Phi(\mu)]]}ds$$
$$+ \sum_{e\subset\partial\Omega} \omega_e \int_e (\partial_n\Phi(\eta)-ik\Phi(\eta))\overline{(\partial_n\Phi(\mu)-ik\Phi(\mu))}ds, \tag{3.8}$$

and the linear form $F(\cdot)$ is given by:

$$F(\mu) = -\sum_{e\text{-interior edge}} \beta_e \int_e [\varphi]\overline{[\Phi(\mu)]}ds - \sum_{e\text{-interior edge}} \gamma_e \int_e [[\partial_n\varphi]]\overline{[[\partial_n\Phi(\mu)]]}ds$$
$$- \sum_{e\subset\partial\Omega} \omega_e \int_e (\partial_n\varphi-ik\varphi-g)\overline{(\partial_n\Phi(\mu)-ik\Phi(\mu))}ds. \tag{3.9}$$

The parameters β_e, γ_e and ω_e are three positive numbers that can be viewed as weight parameters. Note that the third integral in Eqs. (3.8)-(3.9) is theoretically equal to 0 (see the second boundary condition given by BVP1 and BVP2). However, the presence of this term at the algebraic level leads to a more robust and stable formulation. The variational problem (3.7) expresses the continuity in the weak sense of both the solution and its normal derivative. Note that the bilinear form A is Hermitian.

Remark 3.2. Solving BVP and solving the problem arising in the proposed two-step procedure are equivalent in the following sense:

(i) Let $\tilde{u} = \Phi(\lambda) + \varphi$, where for all K, φ^K and $\Phi(\lambda^K)$ are the solutions of (3.2), with λ solution of VF. Then, $\tilde{u}$ is the unique solution of BVP, that is $\tilde{u} = u$.

(ii) Conversely, let u be the solution of BVP. For each $K \in \tau_h$, we define λ by:

$$\lambda^K = \begin{cases} 0, & \text{on } e \subset \partial K \cap \partial\Omega, \\ \partial_n u^K - i\alpha u^K, & \text{on } e \subset \partial K \cap \Omega. \end{cases} \tag{3.10}$$

Using again the standard regularity results for Laplace's operator [14] and the assumptions on the regularity of f and g, we deduce that $\lambda^K \in L^2(\partial K)$, for all $K \in \tau_h$ and therefore $\lambda \in \mathcal{M}$. Let φ^K be the solution of BVP1 and $\Phi(\lambda^K)$ the solution of BVP2. Then, λ is solution of VF and $u = \Phi(\lambda) + \varphi$.

Remark 3.3. The common points, as well as the differences between DGM and mDGM are illustrated in Table 1.

Table 1: Comparison between DGM and mDGM: local and global variational formulation (VF).

Method	DGM	mDGM
Local VF	$\int_{\partial K}(\partial_n w - ikw\mathbb{1}_{\partial K\cap\partial\Omega})\overline{v}=\int_{\partial K\cap\Omega}\mu\overline{v}$	$\int_{\partial K}(\partial_n w - ikw)\overline{v}=\int_{\partial K}\mu\overline{v}$
Global VF	$\displaystyle\sum_{\substack{e\text{-interior}\\ \text{edge}}}\frac{1}{\lvert e\rvert}\int_e[\Phi(\lambda)]\overline{\mu}$ $\displaystyle=-\sum_{\substack{e\text{-interior}\\ \text{edge}}}\frac{1}{\lvert e\rvert}\int_e[\varphi]\overline{\mu}$	$\displaystyle\sum_{\substack{e\text{-interior}\\ \text{edge}}}\beta_e\int_e[\Phi(\lambda)]\overline{[\Phi(\mu)]}$ $\displaystyle+\sum_{\substack{e\text{-interior}\\ \text{edge}}}\gamma_e\int_e[[\partial_n\Phi(\lambda)]]\overline{[[\partial_n\Phi(\mu)]]}$ $\displaystyle+\sum_{e\subset\partial\Omega}\omega_e\int_e(\partial_n\Phi(\lambda)-ik\Phi(\lambda))\overline{(\partial_n\Phi(\mu)-ik\Phi(\mu))}$ $\displaystyle=F(\mu),\quad\text{given by (3.9)}$

4 The algebraic approach

The implementation of mDGM requires first to introduce two finite-dimensional spaces $\mathcal{V}_h$ and $\mathcal{M}_h$ such that $\mathcal{V}_h\subset\mathcal{V}$ and $\mathcal{M}_h\subset\mathcal{M}$. Similarly to the DGM formulation, we have considered spaces of plane waves functions. However, other shape functions satisfying the Helmholtz equation, such as the Bessel functions [19], can also be considered. Moreover, unlike the DGM formulation, mDGM allows - in principle - to choose the spaces $\mathcal{V}_h$ and $\mathcal{M}_h$ independently.

For any element $K\in\tau_h$, we denote by $\mathcal{V}_h(K)$ (resp. $\mathcal{M}_h(K)$) the set of functions of $\mathcal{V}_h$ (resp. $\mathcal{M}_h$) restricted to K (resp. ∂K). Furthermore, n^K (resp. n^{λ^K}) denotes the dimension of $\mathcal{V}_h(K)$ (resp. $\mathcal{M}_h(K)$). Last, the dimension of $\mathcal{M}_h$, which corresponds to the total number of dofs, is denoted by n^λ.

4.1 Step 1: The restriction procedure

For an element $K\in\tau_h$ and for any $\mu_h^K\in\mathcal{M}_h(K)$, we denote by $\varphi_h^K\in\mathcal{V}_h(K)$ and $\Phi_h\left(\mu_h^K\right)\in\mathcal{V}_h(K)$ the approximation of φ^K and $\Phi\left(\mu_h^K\right)$ respectively.

For any element K in the mesh, φ_h, $\Phi_h(\mu_h)$ and μ_h are given by: $\varphi_h|_K=\varphi_h^K$, $\Phi_h(\mu_h)|_K=\Phi_h\left(\mu_h^K\right)$ and $\mu_h|_K=\mu_h^K$.

To compute φ_h and $\Phi_h(\mu_h)$, for all $K\in\tau_h$, we set the variational problem (3.2) in the finite dimensional space $\mathcal{V}_h(K)$, that is:

$$\begin{cases}\text{Find }\Psi_h^K\in\mathcal{V}_h(K)\text{ such that:}\\ a_K\left(\Psi_h^K,v_h^K\right)=L_K\left(v_h^K\right),\quad\forall v_h^K\in\mathcal{V}_h(K),\end{cases}\tag{4.1}$$

where the forms $a_K(\cdot,\cdot)$ and $L_K(\cdot)$ are given by (3.3) and (3.4) - (3.5) respectively, and Ψ_h^K

is the approximation of Ψ^K, solution of the variational problem given by (3.2). Consequently, the variational problem (4.1) can be written in the following matrix form:

$$\left(\mathbf{K}^K - k^2\mathbf{M}^K - i\alpha\mathbf{S}^{\partial K\cap\mathring{\Omega}} - ik\mathbf{S}^{\partial K\cap\partial\Omega}\right)\mathbf{X}^K = \text{rhs}, \tag{4.2}$$

where $\mathbf{K}^K$ (resp. $\mathbf{M}^K$) is the stiffness (resp. mass) matrix at the element level K. $\mathbf{S}^{\partial K\cap\mathring{\Omega}}$ and $\mathbf{S}^{\partial K\cap\partial\Omega}$ are mass-like matrices defined on $\partial K\cap\mathring{\Omega}$ and $\partial K\cap\partial\Omega$ respectively. $\mathbf{X}^K$ is the vector in $\mathbb{C}^{n^K}$ whose components are the coefficients of Ψ_h^K in the basis of $\mathcal{V}_h(K)$.

The linear system (4.2) possesses the following properties:

- All the entries of the corresponding matrix can be evaluated *analytically* for plane waves shape functions.

- The linear system admits a *unique* solution, even when $\partial K\cap\partial\Omega = \varnothing$. Thanks to the positive number α since the presence of the matrix $\mathbf{S}^{\partial K\cap\mathring{\Omega}}$ guarantees the invertibility of the system. Note that this is not the case for the DGM, for which $\mathbf{S}^{\partial K\cap\mathring{\Omega}}$ does not appear, leading to possibly a (weakly) singular system when $\partial K\cap\partial\Omega = \varnothing$.

- The corresponding matrix is neither Hermitian, nor symmetric. This cannot be viewed as a deficiency of the approach since the size of the system is *small* and thus can be solved easily using LU factorization. Indeed, the largest value of the shape functions used so far is $n^K = 64$ (see [9, 10]).

- For an element $K \in \tau_h$, the number of right-hand side is $n^{\lambda^K} + 1$. We must point out that the obtained problems can be solved in parallel since they are independent from an element K to another.

4.2 Step 2: The optimization procedure

In this step, we set the global problem VF in finite dimension. We have:

$$\begin{cases} \text{Find } \lambda_h \in \mathcal{M}_h \text{ such that:} \\ A_h(\lambda_h, \mu_h) = F_h(\mu_h), \quad \forall \mu_h \in \mathcal{M}_h, \end{cases} \tag{4.3}$$

where the forms $A_h(\cdot,\cdot)$ and $F_h(\cdot)$ are obtained from $A(\cdot,\cdot)$ and $F(\cdot)$ respectively by replacing φ with φ_h and $\Phi(\mu_h)$ with $\Phi_h(\mu_h)$, for any $\mu_h \in \mathcal{M}_h$. Hence, solving the variational problem (4.3) comes to solve the following linear algebraic system:

$$\mathbf{A}\boldsymbol{\Lambda} = \mathbf{b}, \tag{4.4}$$

where for each $1 \leq l,m \leq n^\lambda$, $\mathbf{A}_{lm}$ and $\mathbf{b}_l$ are given by $A_h(\mu_m,\mu_l)$ and $F_h(\mu_l)$ respectively. The unknown $\boldsymbol{\Lambda}$ is a vector in $\mathbb{C}^{n^\lambda}$ whose components are the coefficients of λ_h in the basis of $\mathcal{M}_h$. Note that the matrix $\mathbf{A}$ is *Hermitian*. We prove in [3, 13] that the matrix $\mathbf{A}$ is positive semi-definite. In addition, under a compatibility condition, $\mathbf{A}$ is positive definite.

4.3 Computational complexity

Similarly to the DGM formulation designed by Farhat *et al.* in [8–10], the computational cost depends mainly on the number of Lagrange multipliers. Recall that in order to have well-posed local problems we propose in mDGM a complete relaxation of both unknowns: the field and its normal derivative. The discontinuity of the Lagrange multipliers across the interior edges, which does not incur in DGM, is translated at the algebraic level by solving a global system that is two times larger than the one arising in DGM, when using the same element. This is the price to pay to ensure that the matrices at the element level are nonsingular.

5 Numerical investigation

In order to illustrate the potential of mDGM for solving efficiently Helmholtz problems, we have performed numerical experiments using discrete spaces in which the shape functions are plane waves, as done in DGM [8–10]. More specifically, $\mathcal{V}_h$ are the spaces introduced in [8]. Once the local space of shape functions $\mathcal{V}_h(K)$ is chosen, the Lagrange multiplier is approximated on each edge using a subset or all set of shape functions that occur when evaluating $\partial_n v_h^K - i\alpha v_h^K$, for $v_h^K \in \mathcal{V}_h(K)$.

From now on, we suppose that Ω is an $a \times a$ square domain. We use a uniform partition of Ω in rectangular-shaped elements K. The functions f and g are such that the exact solution u of BVP is a plane wave propagating in a direction $\boldsymbol{d} = (\cos\theta, \sin\theta)$. We vary the propagation angle θ in the interval $[0, 2\pi)$. In order to compare the results obtained with mDGM to those delivered by DGM, we measure, for each propagating angle θ, the relative error using the following modified H^1 norm [8]:

$$\|v\|_{\widehat{H^1}} = \left(\sum_K \|v\|_{H^1(K)}^2 + \sum_{e-\text{interior edge}} \|[v]\|_{L^2(e)}^2 \right)^{\frac{1}{2}}, \quad \forall v \in \mathcal{V}. \qquad (5.1)$$

Note that (5.1) is a modified H^1 norm since it takes into account the H^1 norm at the element level and the jump of the numerical solution along the interior interfaces of the mesh. We also use the *total* relative error, that is the *mean* value of the relative error obtained when $\theta \in [0, 2\pi)$.

The results reported in this paper are obtained for $(\beta_e, \gamma_e, \omega_e) = (1, h, h)$. Note that we have investigated numerically the sensitivity of the method to various values of the parameters including $(1,1,1)$ and $(1,1/h,1/h)$ and found that the choice of $(1,h,h)$ delivers the best level of accuracy. Needless to say that a mathematical analysis is paramount to determine the optimal values of $(\beta_e, \gamma_e, \omega_e)$ for ensuring a high level of performance of the proposed method.

We present the results of two classes of numerical experiments: experiments using a lower order element (four plane waves per element), and experiments using higher order

elements (eight and seven plane waves per element). All the results are compared to the ones obtained with DGM.

5.1 Lower order element

For each $K \in \tau_h$, we consider the following discrete local space:

$$\mathcal{V}_h(K) = \left\{ v_h^K = \sum_{1 \leq p \leq 4} e^{ik\boldsymbol{\theta}_p \cdot x} u_p, \ \boldsymbol{\theta}_p = {}^t \left[\cos \theta_p, \sin \theta_p \right], \right.$$

$$\left. \theta_p = \pi/4 + (p-1)\pi/2, \quad 1 \leq p \leq 4, \ u_p \in \mathbb{C} \right\}.$$

The Lagrange multiplier is approximated in the following discrete dual space:

$$\mathcal{M}_h = \left\{ \mu_h \in \mathcal{M}; \quad \forall K \in \tau_h, \quad \mu_h^K|_e = \mu_1^K e^{ik\frac{\sqrt{2}}{2}x} + \mu_2^K e^{-ik\frac{\sqrt{2}}{2}x} \text{ if } e \parallel \overrightarrow{x}, \right.$$

$$\left. \mu_h^K|_e = \mu_1^K e^{ik\frac{\sqrt{2}}{2}y} + \mu_2^K e^{-ik\frac{\sqrt{2}}{2}y} \text{ if } e \parallel \overrightarrow{y}, \quad \mu_1, \mu_2 \in \mathbb{C} \right\},$$

where s represents the curvilinear abscissa. The spaces $\mathcal{V}_h$ and $\mathcal{M}_h$ defined above correspond to the so-called R-4-2 element in the nomenclature of DGM (see [8]). Note that for the DGM, considering two dofs per edge leads also to a complete approximation of the Lagrange multiplier.

The first experiments consist in comparing the error delivered by both numerical methods (DGM and mDGM) for different values of ka, while maintaining kh constant. More specifically, we consider $ka=10$ and $ka=30$ and we choose the step size of the mesh discretization h/a such that $kh=1/5$, which is about 30 elements per wavelength. The results are depicted in Figs. 1 and 2. These results indicate the following:

- The two methods deliver results with the same level of accuracy, as indicated in Fig. 1: both curves are superposed.

- Fig. 2 indicates that the R-4-2 element (for both methods) exhibits little pollution: increasing ka, while maintaining kh constant, leads to an increase in the relative error which is less than 0.5% at most (see Fig. 2 at angles $\theta = l\pi/2$, with $l=0,1,\cdots,8$). Note that these directions are the furthest away from the directions of the shape functions of this element, which explains the maximum errors delivered for the corresponding angles.

Next, we compare the sensitivity of the total relative error (the mean value over the propagation angles) to the mesh size. The result depicted in Fig. 3 is obtained for $ka=1$. One can observe the following:

- For $kh > 1/100$, the errors delivered by the two methods are comparable. The two curves are on top of each other.
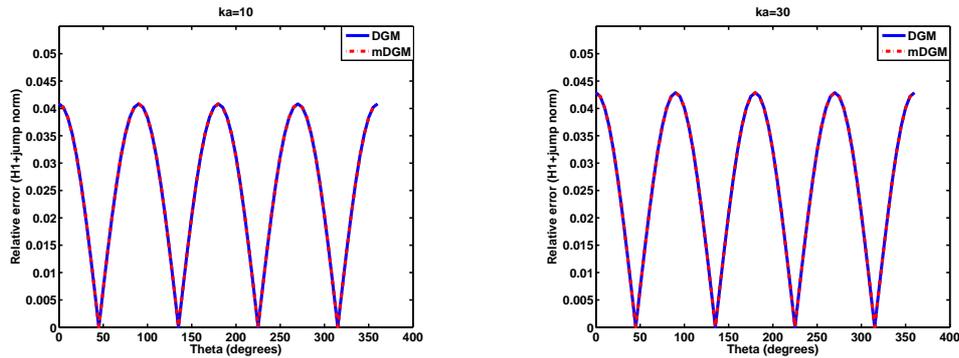
Figure 1: Performance of the two methods for kh=1/5.
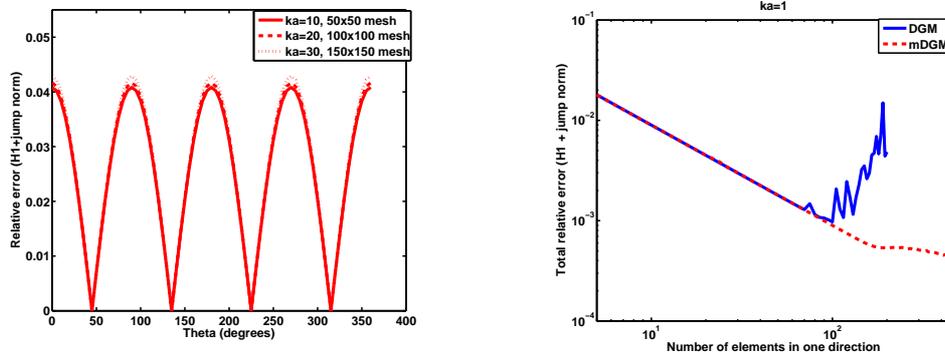
Figure 2: Pollution effect for the R-4-2 element.

Figure 3: Sensitivity of the total relative error with respect to the mesh size for $ka=1$ when using four plane waves.

- For $kh < 1/100$ mDGM outperforms DGM. As we refine the mesh ($kh < 1/100$), DGM becomes unstable. Indeed, there is a dramatic loss in the accuracy of more than one order of magnitude. The error jumps from 0.09% (for $kh=1/100$) to 1.5% (for $kh=1/190$). The instability observed in DGM seems to be related to the severe ill conditioning of the local matrices. Observe that mDGM remains stable as we refine the mesh. The last point of the curve was obtained for $kh=1/450$, the limit of our computing platform. The total relative error for this mesh size is 0.04%.

5.2 Higher order elements

We first approximate the primal variable using eight plane waves, positioned at:

$$\theta_p = (p-1)\pi/4, \quad 1 \le p \le 8. \tag{5.2}$$

For an element $v_h^K \in \mathcal{V}_h(K)$, the full approximation of $\partial_n v_h^K - \mathrm{i} k v_h^K$ leads to five dofs per edge. Note that mDGM can be implemented using less dofs per edge for the Lagrange

multiplier. In the numerical experiments we have considered the following elements:

- R-8-5: $\lambda_h = \mu_1 + \mu_2 e^{iks} + \mu_3 e^{-iks} + \mu_4 e^{ik\frac{\sqrt{2}}{2}s} + \mu_5 e^{-ik\frac{\sqrt{2}}{2}s}$,

- R-8-4: $\lambda_h = \mu_1 e^{iks} + \mu_2 e^{-iks} + \mu_3 e^{ik\frac{\sqrt{2}}{2}s} + \mu_4 e^{-ik\frac{\sqrt{2}}{2}s}$,

- R-8-3: $\lambda_h = \mu_1 + \mu_2 e^{ik\frac{\sqrt{2}}{2}s} + \mu_3 e^{-ik\frac{\sqrt{2}}{2}s}$,

- R-8-2b: $\lambda_h = \mu_1 e^{ik\frac{\sqrt{2}}{4}s} + \mu_2 e^{-ik\frac{\sqrt{2}}{4}s}$.

Note that the R-8-3 element corresponds to the full approximation of the Lagrange multiplier in DGM. In all the experiments, DGM is equipped with the so-called R-8-2b element, which was shown to deliver the most accurate results, when using eight plane waves at the element level [8].

The results depicted in Fig. 4 compare the relative error delivered by both methods, as a function of the propagation angle. More specifically, we have compared DGM equipped with the R-8-2b element to mDGM equipped with each of the R-8-2b, R-8-3, R-8-4 and R-8-5 elements. These results are obtained for $ka = 10$ and $h/a = 1/20$, that is $kh = 1/2$, corresponding to about 12 elements per wavelength. The following observations are noteworthy:

- DGM outperforms mDGM in the case when both methods are equipped with the R-8-2b element (see Fig. 4(a)). This superiority of DGM over mDGM is most likely due to the poor approximation of the Lagrange multiplier in the mDGM (three out of five dofs are neglected), compared to the DGM, where only one dof out of three is neglected.

- The comparison of DGM to mDGM when using 3, 4 and 5 dofs for the Lagrange multipliers (see Figs. 4(b)-(d)) clearly shows the superiority of mDGM over DGM. Indeed, in each of the three cases and for each propagation angle the relative error delivered by mDGM is smaller than the one obtained with DGM. In addition, the total relative error for DGM is about 0.1%, compared to about 0.02% for mDGM equipped with R-8-3, R-8-4 and R-8-5.

Next, we investigate the sensitivity of the total relative error with respect to h, the step size of the mesh discretization. For this, we set $ka = 1$ and we evaluate the total relative error for DGM equipped with the R-8-2b element and for mDGM, when equipped with the R-8-2b, R-8-3, R-8-4 and R-8-5 elements. The results depicted in Fig. 5 illustrate a clear superiority of mDGM over DGM. Indeed, the total relative error obtained with mDGM when using the R-8-2b, R-8-3, R-8-4 and R-8-5 decreases, similarly to DGM, as long as $kh > 1/8$, which corresponds to about 48 elements per wavelength. Then, the total relative error delivered by DGM jumps to 100% for $kh = 1/25$, corresponding to 150 elements per wavelength. In mDGM we observe also an increase in the total relative error as soon as $kh < 1/8$. However, the obtained error does not exceed 1% for $kh > 1/100$, which corresponds to about 600 elements per wavelength.
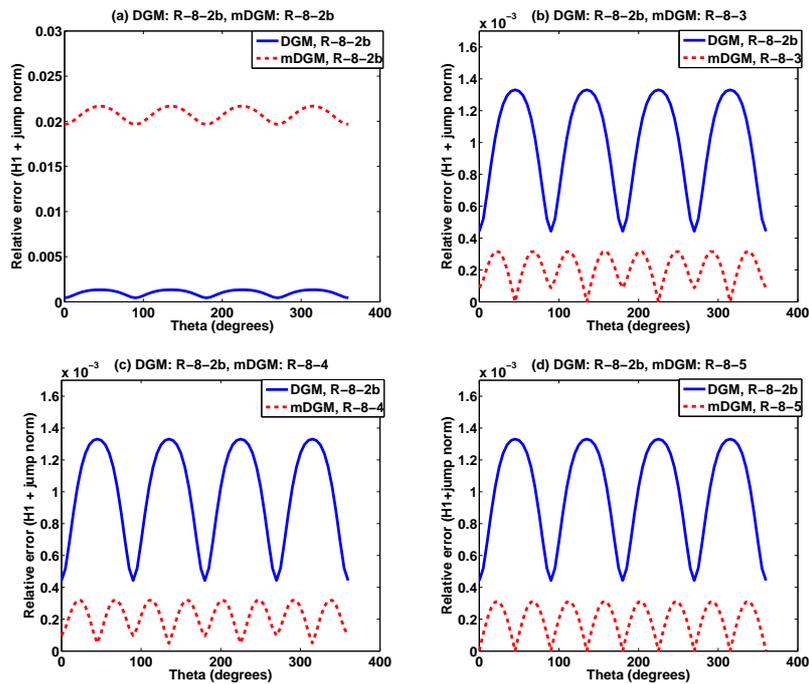
Figure 4: Performance of the two methods when $ka=10$, $h/a=1/20$.
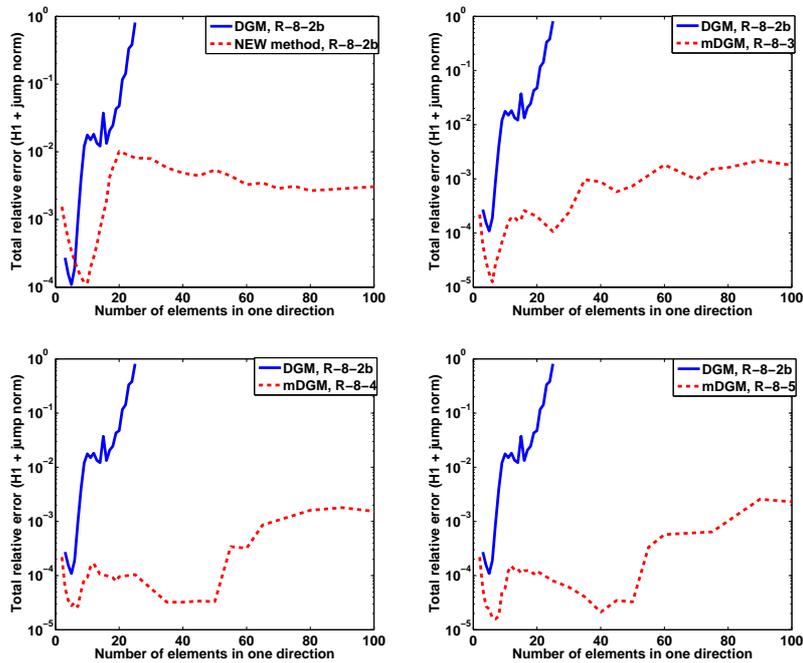
Figure 5: Sensitivity of the total relative error with respect to the mesh size for $ka=1$ when using eight plane waves.
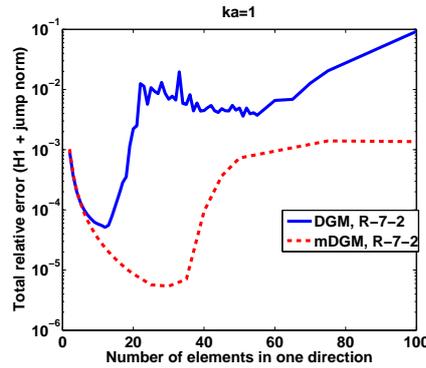
Figure 6: Sensitivity of the total relative error with respect to the mesh size for $ka=1$ when using seven plane waves.

We have shown in [3, 13] that the source of the numerical instabilities observed in mDGM is the numerical loss of the linear independence of the eight shape functions. The following experiment reveals the behavior of mDGM and DGM when the used shape functions remain linearly independent (see [3,13]) as we refine the mesh. This experiment consists in approximating the solution, at the element level, using seven plane waves, positioned at:

$$\theta_p = 2(p-1)\pi/7, \quad 1 \leq p \leq 7. \tag{5.3}$$

We have maintained the same two dofs per edge as in R-8-2b. Following the nomenclature introduced in [8], we will refer to this element as R-7-2. In Fig. 6, we compare the total relative error delivered by the mDGM R-7-2 element to the one obtained when equipping DGM with the R-7-2 element. The following observations are noteworthy:

- The accuracy of the two methods is comparable for $kh > 1/8$. In this region the two curves are superposed.

- The DGM equipped with the R-7-2 element delivers the most accurate approximation (which is about 0.005%) for $kh = 1/12$. Observe that mDGM becomes unstable later: the smallest error (about 0.001%) is obtained for $kh = 1/35$.

- Although for both methods we observe numerical instabilities, mDGM is more accurate than DGM. For any mesh size the error delivered by mDGM is smaller than the one obtained with DGM. Moreover, for some mesh sizes, mDGM outperforms DGM by two orders of magnitude. We believe that this is due to the local problems which are nearly singular in DGM.

6   Summary and conclusion

We have designed a new solution methodology, called mDGM, for Helmholtz problems which is easy to understand and implement. At the element level, we approximate the

solution by a superposition of plane waves. Consequently, the obtained solution is discontinuous and Lagrange multipliers are introduced to ensure the continuity in a weak sense. Unlike the DGM, the Lagrange multiplier is also discontinuous, which allows us to consider well-posed local problems. The algebraic approach requires solving local linear systems with multiple right-hand side: the system's size is given by the number of plane waves considered in the local basis. These problems are independent from one element to another and therefore can be solved in parallel. The global system, whose size is the number of total dofs used for approximating the Lagrange multiplier, is positive semi-definite and Hermitian. The numerical results we have presented show that the proposed method is not only more stable than the DGM, but also exhibits a better level of accuracy. More specifically, as indicated by the reported numerical results, mDGM reduces the level of errors by one to two orders of magnitude depending on the mesh size and on the element.

Acknowledgments

References

[1] M. Amara, H. Barucq, A. Bernardini, R. Djellouli, On the numerical performance of a new discretization scheme for solving Helmholtz problems, Theoretical and Computational Acoustics, M. Taroudakis and P. Papadakis eds. (2008), 139-146.
[2] M. Amara, R. Djellouli, C. Farhat, Convergence analysis of a discontinuous Galerkin method with plane waves and Lagrange multipliers for the solution of Helmholtz problems, SIAM J. Numer. Anal., 47 (2009), 1038-1066.
[3] M. Amara, H. Calandra, R. Djellouli, M. Grigoroscuta-Strugaru, A modified discontinuous Galerkin method for solving Helmholtz problems, Rapport de Recherche, INRIA, 7050, 2009, available online at `http://hal.inria.fr/inria-00421584/fr/`.
[4] I. Babuška, I. J. M. Melenk, The partition of unity method, Int. J. Numer. Meth. Eng., 40 (1997), 727-758.
[5] I. Babuška, S. Sauter, Is the pollution effect of the FEM avoidable for the Helmholtz equation considering high wave numbers?, SIAM J. Numer. Anal., (34) 1997, 2392-2423.
[6] W. Desmet, B. van Hal, P. Sas, D. Vandepitte, A computationally efficient prediction technique for the steady-state dynamic analysis of coupled vibro-acoustic systems, Adv. Engr. Softw., 33 (2002), 527-540.
[7] O. Cessenat, B. Despres, Application of an ultra-weak variational formulation of elliptic PDEs to the two-dimensional Helmholtz problems, SIAM J. Numer. Anal., 35 (1998), 255-299.

[8] C. Farhat, I. Harari, U. Hetmaniuk, A discontinuous Galerkin method with Lagrange multipliers for the solution of Helmholtz problems in the mid-frequency regime, Comput. Methods Appl. Mech. Engr. 192 (2003), 1389-1419.

[9] C. Farhat, P. Wiedemann-Goiran, R. Tezaur, A discontinuous Galerkin method with plane waves and Lagrange multipliers for the solution of short wave exterior Helmholtz problems on unstructured meshes, Wave Motion, 39 (2004), 307-317.

[10] C. Farhat, R. Tezaur, P. Wiedemann-Goiran, Higher-order extensions of a discontinuous Galerkin method for mid-frequency Helmholtz problems, Int. J. Numer. Meth. Eng., 61 (2004), 1938-1956.

[11] L.P. Franca, C. Farhat, A.P. Macedo, M. Lesoinne, Residual-free bubbles for the Helmholtz equation, Int. J. Numer. Meth. Eng., 40 (1997), 4003-4009.

[12] B. V. Genechten, B. Bergen, D. Vandepitte, W. Desmet, A Trefftz-based numerical modeling framework for Helmholtz problems with complex multiple-scatterer configurations, J. Comput. Phys., 229 (2010), 6623-6643.

[13] M. Grigoroscuta-Strugaru, Contribution à la résolution numérique des problèmes de Helmholtz, University of Pau, France, December 2009, available online at http://tel.archives-ouvertes.fr/index.php?halsid=6lbpnng9qev5snpremhtjku7o7&view_this_doc=tel-00473486&version=2

[14] P. Grisvard, Elliptic Problems in Nonsmooth Domains Pitman, Boston, 1985

[15] J. Hadamard, Lectures on Cauchy's Problem in Linear Partial Differential Equations, Yale University Press, New Haven, 1923.

[16] L. Hörmander, The Analysis of Linear Partial Differential Operator, Springer-Verlag, New York, 1985.

[17] F. Ihlenburg, Finite Element Analysis of Acoustic Scattering, Appl. Math. Sci., 132, Springer-Verlag, New York, 1998.

[18] F. Magoulès, Computational Methods for Acoustics Problems, Saxe-Coburg Publications, 2008.

[19] P. Monk, D. Q. Wang, A least-squares method for the Helmholtz equation, Comput. Methods Appl. Mech. Eng., 175 (1999), 121-136.

[20] M. E. Rose, Weak element approximations to elliptic differential equations, Numer. Math., 24 (1975), 185-204.

[21] O. Schenk, K. Gärtner, Solving unsymmetric sparse systems of linear equations with PARDISO, J. Future Generation Comp. Sys., 20 (2004), 475-487.

[22] O. Schenk, K. Gärtner, On fast factorization pivoting methods for symmetric indefinite systems, Elec. Trans. Numer. Anal., 23 (2006), 158-179.

[23] M. Stojek, Least-squares Trefftz-type elements for the Helmholtz equation, Int. J. Numer. Meth. Eng., 41 (1998), 831-849.

[24] M. E. Taylor, Partial Differential Equations I: Basic Theory, Springer-Verlag, New York 1997.